Electron-rotation coupling in diatomics under strong-field excitation

Yan Rong Liu,[1] Yong Wu,[2,3] Jian Guo Wang,[2] Oriol Vendrell,[4] Victor Kimberg,[5,6,7] and Song Bin Zhang[1,*]

[1]*School of Physics and Information Technology, Shaanxi Normal University, Xi'an 710119, China*

[2]*Institute of Applied Physics and Computational Mathematics, P.O. Box 8009, Beijing 100088, China*

[3]*Center for Applied Physics and Technology, Peking University, Beijing 100084, China*

[4]*Theoretische Chemie, Physikalisch-Chemisches Institut, Universitat Heidelberg, Im Neuenheimer Feld 229, 69120 Heidelberg, Germany*

[5]*Theoretical Chemistry and Biology, Royal Institute of Technology, Stockholm 10691, Sweden*

[6]*Siberian Federal University, 660041 Krasnoyarsk, Russia*

[7]*Kirensky Institute of Physics, Federal Research Center KSC SB RAS, 660036 Krasnoyarsk, Russia*

(Received 23 June 2020; accepted 8 September 2020; published 29 September 2020)

The photoexcitation and photodissociation of diatomic molecules by intense pulse lasers has been the subject of extensive investigations over the past decades. However, the usually employed theoretical framework neglects the coupling between the molecular rotational angular momentum (**R**) and the angular momentum of the electrons projected onto the molecular axis $\Omega = \Lambda + \Sigma$, which results in the known Λ-doubling phenomenon in high-resolution electronic spectra of diatomic molecules. While neglecting this coupling is an excellent approximation in the weak-field or perturbative regime owing to the large mass difference between the rotating atoms and the electrons, the approximation breaks down for intense laser pulses because of the repeated Rabi cycling of the electronic transitions, which can have a significant effect on the rotational degrees of freedom of the molecule. By correcting the transition dipole matrix elements and introducing angular basis sets based on Wigner D functions, the conventional theoretical treatment is generalized to a universal description valid for both the weak- and strong-field regimes. The theoretical treatment developed here is applied to the $|^1\Sigma\rangle$ to $|^1\Pi\rangle$ transitions in diatomic systems. Our results reveal that, for field intensities resulting in about one Rabi cycling for extreme ultraviolet or x-ray transitions, the theoretical predictions by the conventional theoretical frame need to be corrected when considering observables such as the molecular alignment and the angular distribution of the photofragments.

DOI: 10.1103/PhysRevA.102.033114

I. INTRODUCTION

Owing to the continuous development of ultrashort and intense infrared (IR) laser sources, strong-field physics has yielded impressive results over the past decades [1–4]. Many applications of light-induced ultrafast nonlinear dynamics in atoms and molecules have been discovered, such as high harmonic generation (HHG) [5–8], molecular field-free alignment [9–12], transient absorption spectroscopy [13–15], resonance manipulation [16–18], and ionization-dissociation [19–21]. Using pump-probe schemes based on such technologies, the real-time electronic-nuclear dynamics of molecules could be followed with unprecedented details [2,22,23]. The more recent development of x-ray free-electron laser (XFEL) facilities provides access to femtosecond pulses of gigawatt peak intensity in the soft-x-ray range [24–30] and extends the pump-probe schemes from mainly vibrational and electronic excitation with IR pulses to electronic excitation of valence and core-to-valence transitions in the extreme ultraviolet (XUV) and x-ray ranges, thus opening the door to new opportunities to investigate the coupled electron-nuclear dynamics in molecules [26,31–35].

The theoretical treatment of the coupling between vibrational and electronic degrees of freedom is nowadays well understood [36,37] and recent theoretical works have proposed the application of transient absorption [38] and other nonlinear techniques to probe these dynamics [39,40]. On the other hand, the nonadiabatic coupling between rotational and electronic degrees of freedom induced by external electromagnetic fields may need to be revised to consider the direct interaction of the electronic and rotational angular momenta. The coupling between electronic and rotational degrees of freedom becomes important in the description of light-induced conical intersections [41], which are an eminently nonperturbative phenomenon, and in other phenomena concerning the rotational degrees of freedom of molecules in strong fields, such as in molecular alignment and orientation [9]. The usual treatment of these strong-field phenomena involves the coupling of electronic and rotational degrees of freedom at the level of the angular dependence of the transition-dipole moments between electronic states in the laboratory frame after invoking the Born-Oppenheimer approximation. In this level of description, the coupling arises from the different potential energy of the molecule depending on the populated electronic state at a given orientation. It misses, however, the direct angular-momentum coupling, which has a kinetic origin. In the present paper we investigate

*song-bin.zhang@snnu.edu.cn

strong-field phenomena related to the coupling of electronic and rotational degrees of freedom in diatomic molecules and show how, in the case of molecules dressed by a strong laser field, the proper treatment of the coupling becomes crucial for a correct description of some rotation-related observables.

We apply this theory to the case of a diatomic molecule interacting with a strong laser resonant with the transition between the $|^1\Sigma\rangle$ and $|^1\Pi\rangle$ states [42,43]. Typically, the molecular rotations are conventionally described in a basis of spherical harmonics and Legendre polynomials [9,10]. This approach, however, fails to properly describe molecular dynamics in the strong field due to the missing coupling between the molecular rotational angular momentum (**R**) and the electronic interior angular momentum projected onto the molecular axis, $\Omega = \Lambda + \Sigma$ (**R**-Ω coupling). Instead, the exact theoretical description based on the use of Wigner D functions has to be applied [44]. As we show in the present paper, this treatment is also important for the case where the $|^1\Sigma\rangle$ and $|^1\Pi\rangle$ electronic states are coupled via strong vacuum ultraviolet (VUV) fields. Our work illustrates the importance of **R**-Ω coupling for photoexcitation and photodissociation processes associated with intense laser pulses in molecules. Note that the coupling of angular momenta in atoms is quite general, the decoupling of them causes the changes of selection rules in high electromagnetic field [45,46].

The numerical results compare the usual theory ignoring **R**-Ω coupling and using spherical harmonics (or Legendre polynomials) with the theory using the correct transition dipole operators and Wigner D functions. Non-negligible differences are found in various observables such as excited-state populations, molecular alignment, and the angular distribution of the photofragments, as soon as the applied UV field is strong enough to induce more than one Rabi cycle.

II. THEORY AND COMPUTATIONAL DETAILS

In the dipole approximation, the photon-matter interacting operator $\mathbf{O}$ in the space-fixed (SF) axis (indicated by superscript s) is $\mathbf{O}^s = \vec{\boldsymbol{\varepsilon}}^{\,s} \cdot \vec{\boldsymbol{\mu}}^s$, where $\vec{\boldsymbol{\varepsilon}}$ is the electric field and $\vec{\boldsymbol{\mu}}$ is the dipole operator consisting of transition dipole matrix elements [48]. For molecular systems, $\vec{\boldsymbol{\mu}}^s$ is not equal to $\vec{\boldsymbol{\mu}}^m$ in the molecular-fixed (MF) axis (indicated by the superscript m) but can be transformed as $\vec{\boldsymbol{\mu}}^s = \mathbf{D}(\alpha\beta\gamma)\vec{\boldsymbol{\mu}}^m$, where $\mathbf{D}(\alpha\beta\gamma)$ is the rotation operator connecting the SF and MF frames, α and γ are the Euler angles representing rotations around the SF Z axis and MF z axis, respectively, and β is the Euler angle between the SF Z axis and MF z axis (see Fig. 1) [48]. With the tensors defined as $\mathrm{T}^1_0(\vec{\boldsymbol{\varepsilon}}^{\,s}) = \varepsilon^s_Z$, $\mathrm{T}^1_{\pm1}(\vec{\boldsymbol{\varepsilon}}^{\,s}) = \mp\frac{1}{\sqrt{2}}(\varepsilon^s_X \pm i\varepsilon^s_Y)$, $\mathrm{T}^1_0(\vec{\boldsymbol{\mu}}^m) = \mu^m_z$, and $\mathrm{T}^1_{\pm1}(\vec{\boldsymbol{\mu}}^m) = \mp\frac{1}{\sqrt{2}}(\mu^m_x \pm i\mu^m_y)$, $\mathbf{O}^s$ can be explicitly written as [48,49]

$$\mathbf{O}^s = \mathbf{T}^1(\vec{\boldsymbol{\varepsilon}}^{\,s}) \cdot \mathbf{T}^1(\vec{\boldsymbol{\mu}}^s) = \sum_{p=-1}^{1}\sum_{q=-1}^{1}(-1)^q \mathrm{T}^1_{-p}(\vec{\boldsymbol{\varepsilon}}^{\,s})\mathrm{T}^1_q(\vec{\boldsymbol{\mu}}^m)\mathrm{D}^1_{p,q}(\alpha\beta\gamma), \quad (1)$$

where $\mathrm{D}^1_{p,q}(\alpha\beta\gamma)$ is the Wigner D function, the matrix elements of the rotational operator $\mathbf{D}(\alpha\beta\gamma)$. In the case of a linearly polarized laser with polarization in SF Z axis (the case of $p = 0$), Eq. (1) simplifies as

$$\mathbf{O}^s(p=0) = \varepsilon^s_Z\left(\frac{\mu^m_x + i\mu^m_y}{\sqrt{2}}\frac{\sin\beta}{\sqrt{2}}e^{i\gamma} + \mu^m_z\cos\beta + \frac{\mu^m_x - i\mu^m_y}{\sqrt{2}}\frac{\sin\beta}{\sqrt{2}}e^{-i\gamma}\right). \quad (2)$$

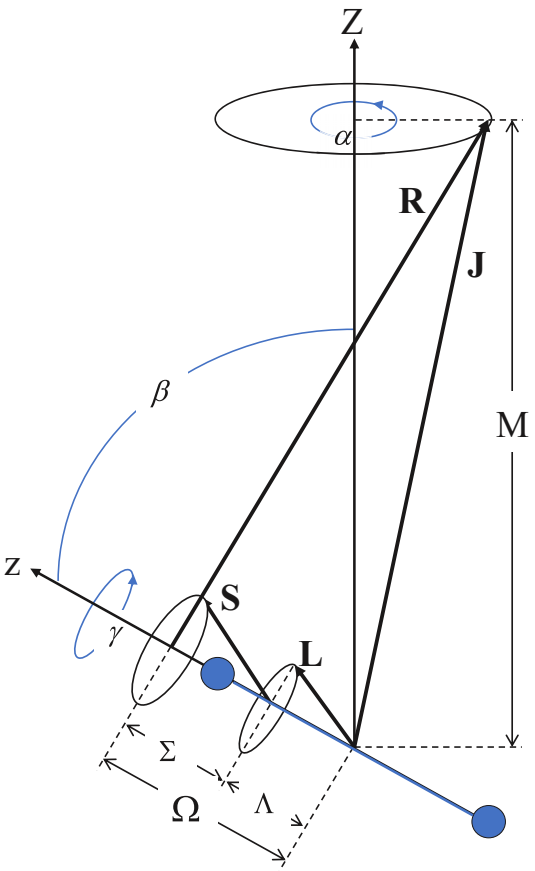

FIG. 1. Schematics of Hund's case-(a) coupling. The same convention as in Zare [47] is used to name the various quantities.

Using Hund's case-(a) (see Fig. 1) and the Born-Oppenheimer approximation, the total wave function of a diatomic molecule can be explicitly written as $\Psi = |\phi\chi; \mathrm{J}, \mathrm{M}, \Omega\rangle$ [47–49], where M is the projection of the total angular momentum **J** onto the SF Z axis and **R** is the rotational angular momentum; the projection of **J** onto the molecular axis (MF z axis) or the total interior angular momentum about the z axis is $\Omega = \Lambda + \Sigma$, where Λ and Σ are the projections of the total orbital angular momentum **L** and spin angular momentum **S** onto the molecular axis, respectively; and $|\phi\rangle$, $|\chi\rangle$, and $|\mathrm{J}, \mathrm{M}, \Omega\rangle = (\frac{2\mathrm{J}+1}{8\pi^2})^{1/2}\mathrm{D}^{\mathrm{J}}_{\mathrm{M},\Omega}(\alpha\beta\gamma)$ represent the electronic, vibrational, and rotational parts, respectively [47,50]. For the electronic transitions from $|\phi_i\rangle$ to $|\phi_f\rangle$, when $\Delta\Lambda_{f\leftarrow i} = 0$, only the second term of Eq. (2) is nonzero and the transition dipole moment is $\mu^{\parallel}_{f\leftarrow i} = \langle\phi_f|\mu^m_z|\phi_i\rangle$; the first term of Eq. (2) describes transitions with $\Delta\Lambda_{f\leftarrow i} = +1$ and the transition dipole moment is $\mu^{\perp}_{f\leftarrow i} = \langle\phi_f|\frac{\mu^m_x + i\mu^m_y}{\sqrt{2}}|\phi_i\rangle$; the

reverse transitions with $\Delta\Lambda_{i\leftarrow f}=+1$ or $\Delta\Lambda_{f\leftarrow i}=-1$ and the transition dipole moment $\mu^{\perp}_{i\leftarrow f}=(\mu^{\perp}_{f\leftarrow i})^{\dagger}=\langle\phi_i|\frac{\mu^m_x-i\mu^m_y}{\sqrt{2}}|\phi_f\rangle$ correspond to the third term of Eq. (2). Note that, in Eq. (2), only one term is nonzero for any matrix element between two electronic basis functions [49].

Let us now consider a diatomic molecule of reduced mass μ whose two well-separated electronic states $|11\rangle$ and $|22\rangle$ with potential-energy curves $V_{11}(q)$ and $V_{22}(q)$ are resonantly coupled by a linearly polarized laser, and where q is the internuclear distance. The nuclear Hamiltonian $\mathbf{H}(\mathbf{q})$ for the system can be written as

$$\mathbf{H}(\mathbf{q})=\mathbf{T}(q)+\frac{\mathbf{R}^2}{2\mu q^2}+\begin{pmatrix}V_{11}(q)+\mu_{11}(q)\varepsilon(\omega,t)\kappa_{11}(\beta\gamma) & (V_{\Sigma-\Sigma'})^{\dagger}\\ V_{\Sigma-\Sigma'} & V_{22}(q)+\mu_{22}(q)\varepsilon(\omega,t)\kappa_{22}(\beta\gamma)\end{pmatrix}, \tag{3}$$

where $\mathbf{T}(q)$ is the kinetic operator, $\mathbf{R}^2=\mathbf{J}^2-\Omega^2$ [47,48], $V_{\Sigma-\Sigma'}=\mu_{21}(q)\varepsilon(\omega,t)\kappa_{21}(\beta\gamma)$ (the subscript Σ indicates the electronic states $|\Sigma\rangle$). $\kappa_{fi}(\beta\gamma)=\cos\beta$ or $\frac{\sin\beta}{\sqrt{2}}e^{i\gamma}$ for $\Delta\Lambda_{f\leftarrow i}=0$ or $+1$, respectively [see. Eq. (2)]. The off-diagonal term $V_{\Sigma-\Sigma'}$ of Eq. (3) corresponds to the photon-molecule transition dipole interaction (coupling). The potentials are far away from each other, the diabatic coupling between them is small and not included in the off-diagonal term. The linear Stark effect (Stark-shift term in the diagonal) is small for UV or x-ray transitions due to the rapid oscillating averages and can be safely neglected [51–53]. The linear Stark effect can be important in high-frequency fields when the interaction time is less than the field period, as the tunneling ionization of molecules [54,55]. The dynamics of the nuclear wave packet $\Phi(\mathbf{q},t)=[\Phi_{11}\ \Phi_{22}]^{\mathrm{T}}$ of the system can be found from the numerical solution of the corresponding Schrödinger equation with Hamiltonian (3) and initial conditions $\Phi(\mathbf{q},t=0)=[\Phi_{11}(t=0)\quad 0]^{\mathrm{T}}$ and $|\Phi_{11}(t=0)\rangle=|\chi_{11};J^0_{11},M,\Omega\rangle$ using the basis expansions, in particular the L_2-normalized Wigner D functions $|J,M,\Omega\rangle=(\frac{2J+1}{8\pi^2})^{1/2}D^J_{M,\Omega}(\alpha\beta\gamma)$ for the angular part.

For the initial nuclear wave function $|\Phi_{11}(t=0)\rangle$ on $|11\rangle$, the electronic state (labeled as $^{2s^0_{11}+1}|\Lambda^0_{11}|$) is Λ doubling with $(2-\delta_{0,\Lambda^0_{11}})$ degrees of degeneracy, the spin projection (Σ) and quantum number (M) have $(2S^0_{11}+1)$ and $(2J^0_{11}+1)$ degrees of degeneracy, respectively, so the total degeneracy for the initial state $|11\rangle$ is $D_{11}=\sum_\Omega\sum_M=\sum_{\Sigma=-S^0_{11}}^{S^0_{11}}\sum_{\Lambda=-\Lambda^0_{11}}^{\Lambda^0_{11}}\sum_{M=-J^0_{11}}^{J^0_{11}}=(2S^0_{11}+1)(2-\delta_{0,\Lambda^0_{11}})(2J^0_{11}+1)$ [56]. An operator for the physical observables generally should be varied with respect to q, β, and t as $\mathbf{O}(q\beta t)$ in order to predict its expectation value $\overline{\mathbf{O}}_{ii}(\Sigma\Lambda M)$ in the electronic state $|ii\rangle$, the final numerical results must be averaged over the degenerate initial states as $\overline{\overline{\mathbf{O}}}_{ii}=\frac{1}{D_{11}}\sum_\Omega\sum_M\overline{\mathbf{O}}_{ii}(\Sigma\Lambda M)$. The universal theoretical framework proposed for the strong-field mediated coupling of electronic and rotational degrees of freedom consists of the solutions of the Schrödinger equation with Hamiltonian (3) together with the averaging over the initial degenerate states. For a thermal system with a finite temperature, the model can be easily extended by averaging the rotational states from different J involving the Boltzmann weights. For experiments at large rotational temperatures, thermal averaging of the initial J states must be taken into account in the standard way [57–59]. In the rest of the work, we suppose the molecular temperature is quite low.

For the weak-field case, first-order perturbation theory can still be applied. In this case, the nuclear wave function of the excited state $|22\rangle$ is given by the product of the electronic transition dipole and the initial wave function of state $|11\rangle$ as $|\Phi_{22}(t)\rangle\propto\kappa_{21}(\beta\gamma)|J^0_{11},M_{11},\Omega_{11}\rangle$. Hence, it is easy to get the quantity $\overline{\mathbf{O}}_{22}(\Sigma\Lambda M)\propto\langle J^0_{11},M,\Omega|\kappa_{21}(\beta\gamma)^{\dagger}\mathbf{O}(q\beta t)\kappa_{21}(\beta\gamma)|J^0_{11},M,\Omega\rangle$. By using the summation relationship between the Winger D functions and the spherical harmonics as $\sum_M|D^J_{M,\Omega}\rangle\langle D^J_{M,\Omega}|=\frac{4\pi}{2J+1}\sum_M|Y^J_M\rangle\langle Y^J_M|$, this results in the relationship

$$\overline{\overline{\mathbf{O}}}_{22}\propto\frac{1}{D_{11}}\sum_\Omega\sum_M\left\langle J^0_{11},M,\Omega\middle|\kappa_{21}(\beta\gamma)^{\dagger}\mathbf{O}(q\beta t)\kappa_{21}(\beta\gamma)\middle|J^0_{11},M,\Omega\right\rangle \tag{4a}$$

$$\simeq\frac{2\pi}{2J^0_{11}+1}\sum_M\left\langle J^0_{11},M\middle|\kappa_{21}(\beta\gamma=0)^{\dagger}\mathbf{O}(q\beta t)\kappa_{21}(\beta\gamma=0)\middle|J^0_{11},M\right\rangle \tag{4b}$$

$$\simeq 2\pi\left\langle J^0_{11}=0,M=0\middle|\kappa_{21}(\beta\gamma=0)^{\dagger}\mathbf{O}(q\beta t)\kappa_{21}(\beta\gamma=0)\middle|J^0_{11}=0,M=0\right\rangle, \tag{4c}$$

after averaging over the degenerate initial states, where $|J,M\rangle=Y^J_M(\beta\alpha)$ is the spherical harmonic and $|J,M=0\rangle=P_J(\beta)$ is the Legendre polynomial [47]. Equations (4a)–(4c) show mathematically two consecutive approximations [Eqs. (4b) and (4c)] of the exact theoretical treatment [Eq. (4a)]. Note that the approximations come from the minor different rotational level shifting between the two electronic states, which would result in little difference in the rovibrational transition strength.

In Eq. (4b) the **R**-Ω coupling is neglected (letting $\Omega=\Lambda=\Sigma=\gamma=0$ and $J=R$) and spherical harmonics $|J=R,M\rangle$ are employed [Eq. (4b)]. In Eq. (4c) Legendre polynomials $|J=R,M=0\rangle$ are used as the angular basis sets for the special initial case of $J=M=0$, resulting in a

degeneracy of the initial state of the system for the approximate treatments of $(2J^0_{11}+1)$ and 1, respectively, independent on Λ and Σ or Ω. These two simplified treatments letting $\gamma = 0$, decoupling $\mathbf{R}$ and Ω and using spherical harmonics to describe the rotational dynamics [60–62], especially the latter one using Legendre polynomials to describe the rotational dynamics, have been conventionally employed by many groups to study photoinduced transitions in molecules for electronically resolved quantities, even for intense laser pulses [41–43,63–71]. Apparently, such conventional treatments can be safely implemented for weak-field interactions, since the weak field hardly alters the rotational state of $|11\rangle$ after averaging over its initial degenerate levels D_{11}, and only the direct-interaction energy resulting from the β-dependent transition dipole moment contributes to the rotational excitations for the system in the excited electronic state $|22\rangle$.

For the intense pulse interactions, especially when involving Rabi cycling, perturbation theory cannot be employed and the approximation of Eqs. (4b) and (4c) to (4a) does not remain valid any more. The transition between states $|11\rangle$ and $|22\rangle$ involves a direct coupling with the molecular rotation in addition to the one arising from the β-dependent transition dipole moment. The accumulated coupling effect during the Rabi cycling driven by the intense field becomes non-negligible and cannot be captured anymore by the usual conventional theoretical treatments that neglect this type of coupling, so the universal treatment of Eq. (3) should be fully employed.

In a short summary, for the transition from state $|\Sigma\rangle$ to $|\Pi\rangle$, in the conventional theoretical treatment, the electron-rotational coupling is neglected, the term of transition dipole interaction does not depend on Ω, Λ, and γ, the angular basis functions are described by Legendre polynomials [50] as

$$\begin{cases} |\mathrm{J}=\mathrm{R},\mathrm{M}=0\rangle = \mathrm{P_J}(\beta), \\ \mathrm{V}_{\Sigma-\Pi} = \mu_{21}(\mathrm{q})\varepsilon(\omega,t)\frac{\sin\beta}{\sqrt{2}}, \end{cases} \tag{5}$$

and the present full treatment includes the electron-rotational coupling, Ω, Λ, and γ fully involve the transitions and the rotational dynamics are described by the L_2-normalized Wigner D functions [50] as

$$\begin{cases} |\mathrm{J},\mathrm{M},\Omega\rangle = \left(\frac{2\mathrm{J}+1}{8\pi^2}\right)^{1/2}\mathrm{D}^{\mathrm{J}}_{\mathrm{M},\Omega}(\alpha\beta\gamma), \\ \mathrm{V}_{\Sigma-\Pi} = \mu_{21}(\mathrm{q})\varepsilon(\omega,t)\frac{\sin\beta}{\sqrt{2}}e^{i\gamma} \end{cases}. \tag{6}$$

By carefully studying the results from different theoretical treatments, the next section discusses the effect of electron-rotation coupling in diatomics by strong field.

III. RESULTS AND DISCUSSIONS

To illustrate the importance of the proposed theoretical approach, we consider the case of photoinduced transitions involving the electronic states $|^1\Sigma\rangle$ and $|^1\Pi\rangle$ of a diatomic molecule in both the approximated conventional and the proposed full theoretical treatments. For comparison, common physical quantities such as electronic state populations, molecular alignment, kinetic-energy release (KER) spectra, and the angular distribution of photofragments are analyzed. We show how, in the case where the laser field is strong enough to drive more than one Rabi cycle on the considered molecular transition, the nuclear dynamics predicted by the conventional treatment differ from the improved theory. The difference is especially pronounced when the upper state has dissociative character: the angular distribution of the photofragments shows clearly different profiles, and the differences become more significant with the increase of the laser intensity.

Figures 2(a) and 3(a) show the model potential-energy curves of the diatomic molecule ($\mu = 1$ AMU) for the two typical cases of bound-bound and bound-dissociative $|\Pi\rangle \leftarrow |\Sigma\rangle$ transitions, respectively, along with a schematic representation of the ground- and excited-state nuclear wave packets. In the present calculations, the terms of dynamic Stark shift in Hamiltonian (3) are neglected and the transition dipole moment is considered within the Condon approximation to be constant $\mu_{21}(\mathrm{q}) \equiv \mu_{21}$, which more clearly highlights the effects of the $\mathbf{R}$-Ω coupling. The resonant laser field consists of a 50 fs sin-squared pulse with central frequency $\omega = 10$ eV and the peak of electric-field amplitude envelope ε_0 defined by the Rabi frequency $\Omega_{\mathrm{Rabi}} = \mu_{21}\varepsilon_0$ [18,72] varied from 0.01 to 0.6 eV. Note that the Rabi period for $\Omega_{\mathrm{Rabi}} = 0.165$ eV is about 50 fs.

The simulations are performed by using the multiconfigurational time-dependent Hartree method (MCTDH) [50] as implemented in the Heidelberg package [73]. For the vibrational degree of freedom, 91 and 291 sin-DVR basis elements were distributed in the internuclear coordinate range [1.0, 10.0] and [1.0, 30.0] a.u. for the cases of bound-bound and bound-dissociative transitions, respectively. A complex absorbing potential (CAP) with form $-iW(\mathrm{q}) = -i\eta(\mathrm{q}-\mathrm{q}_0)^3$ was applied to calculate the photodissociation in the bound-dissociative case through flux analysis [42], with intensity $\eta = 2\times10^{-4}$ a.u. and $\mathrm{q}_0 = 20$ a.u. The rotational degree of freedom β was expanded by using 51 Legendre polynomial basis functions in the conventional treatment, and by L_2-normalized Wigner D functions in the improved theoretical framework; 11 exp-DVR for γ and one k-DVR for α in the Wigner D functions were used. For the case of the bound-bound transitions, we consider the electronic states populations $\mathrm{P}_{ii}(t) = \langle\Phi_{ii}(t)|\Phi_{ii}(t)\rangle$ and the molecular alignment defined as $\langle\cos^2\rangle_{ii}(t) = \langle\Phi_{ii}(t)|\cos^2\beta|\Phi_{ii}(t)\rangle\mathrm{P}^{-1}_{ii}(t)$, where ii stands for 11 (Σ) and 22 (Π) states, respectively. For the case of bound-dissociative transitions, the KER spectra $\mathrm{P}^{22}_{\mathrm{KER}}(E)$ and the angular distribution of photofragments $\mathrm{P}^{22}_{\mathrm{angle}}(\beta_j)$ of the upper dissociative state $|\Pi\rangle$ were calculated from the CAP as [50,74]

$$\begin{cases} \mathrm{P}^{22}_{\mathrm{KER}}(E) = \frac{1}{\pi}\left\{\int_0^\infty\int_0^\infty\langle\Phi_{22}(t)|W|\Phi_{22}(t')\rangle e^{-iE(t-t')}dtdt'\right\} \\ \mathrm{P}^{22}_{\mathrm{angle}}(\beta_j) = \frac{1}{w_j}\int_0^\infty dt\langle\Phi_{22}(t)|W_{\beta_j}|\Phi_{22}(t)\rangle \end{cases}, \tag{7}$$

where $-iW_{\beta_j} = -i[w_j^{1/2}\chi_p(\beta_j)]^*W[w_j^{1/2}\chi_p(\beta_j)]$ is the projection of the CAP to a specific angle β_j of the angular DVR $\chi_p(\beta)$ with the associated weight w_j to this grid point [42,74]. The DVRs satisfy the relations of discrete orthonormality $\sum_j w_j\chi_p(\beta_j)^*\chi_q(\beta_j) = \delta_{pq}$ and discrete completeness $\sum_p(w_jw_{j'})^{1/2}\chi_p(\beta_j)^*\chi_p(\beta_{j'}) = \delta_{jj'}$ [50]. Obviously, the total yield of the photofragments

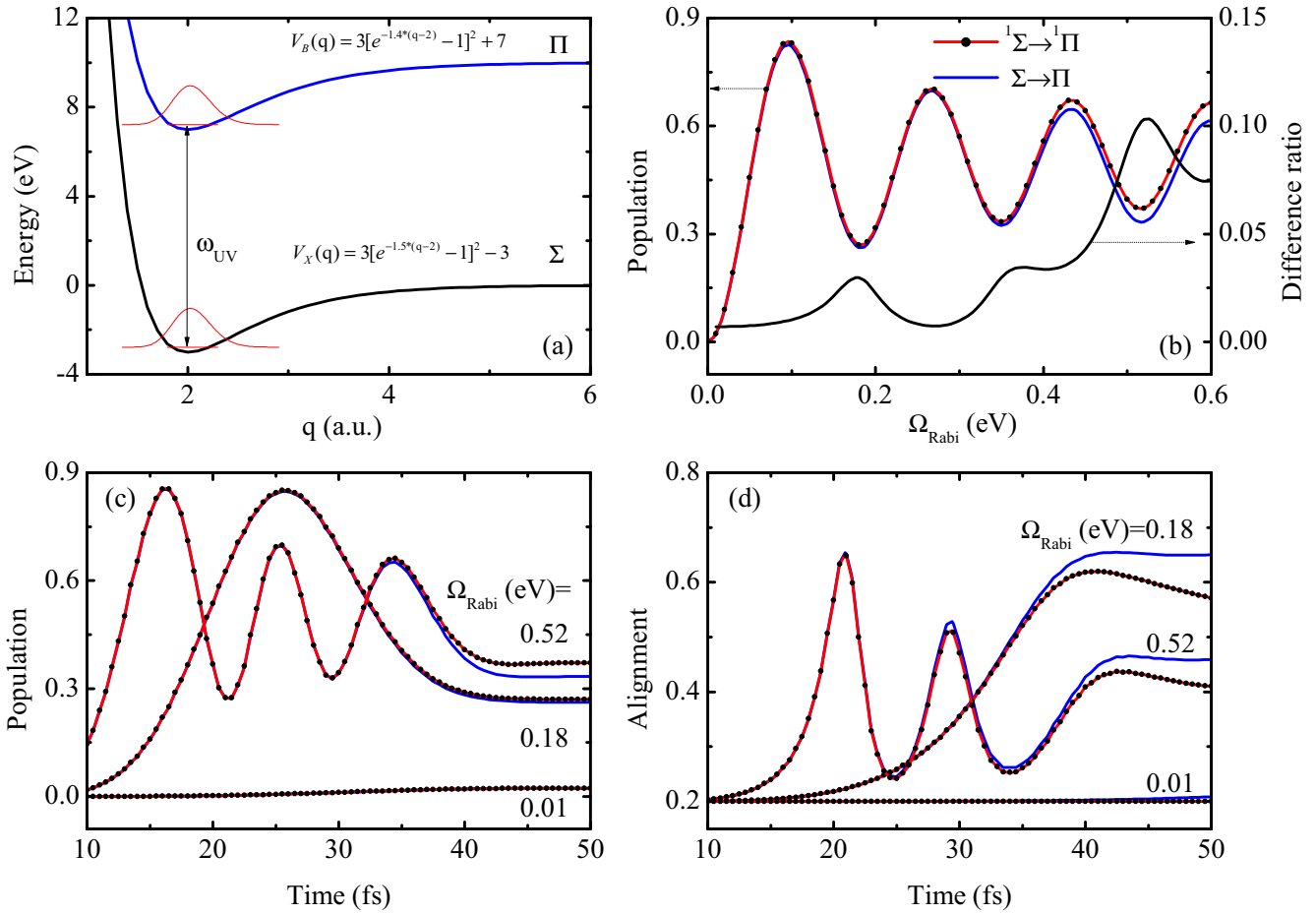

FIG. 2. (a) Potential-energy curves for the electronic transitions from the ground state $|^1\Sigma\rangle$ to a bound excited state $|^1\Pi\rangle$. (b) The dynamics of the upper electronic state population simulated by the conventional ("$\Sigma - \Pi$") and full ("$^1\Sigma - {}^1\Pi$") theoretical treatments with respect to the Rabi frequency Ω_{Rabi} are shown by blue and red-dotted curves, respectively. The ratio of the population difference $[(P_{^1\Sigma - {}^1\Pi} - P_{\Sigma-\Pi})/P_{^1\Sigma - {}^1\Pi}]$ between the two treatments is shown in black. (c), (d) Dynamics of time-dependent population and alignment of the upper electronic state for selected cases with $\Omega_{\text{Rabi}} = 0.01$, 0.18, and 0.52 eV, respectively.

equals $P^{22}_{\text{diss}} = \int P^{22}_{\text{KER}}(E)dE = \int P^{22}_{\text{angle}}(\beta)\sin\beta d\beta = 2\int_0^\infty dt\,\langle\Phi_{22}(t)|W|\Phi_{22}(t)\rangle$.

Figures 2(b)–2(c) and 3(b)–3(c) show the photoexcitation and dissociation properties for the cases of bound-bound [Fig. 2(a)] and bound-dissociative [Fig. 3(a)] transitions, respectively. The curves labeled "$\Sigma - \Pi$" correspond to the conventional calculations that ignore the **R**-Ω coupling and use Legendre polynomials as the angular basis from initial state $|\Sigma\rangle$ with $|R^0_\Sigma = 0, M_\Sigma = 0\rangle$; the curves labeled "$^1\Sigma - {}^1\Pi$" indicate the calculations with the improved treatment considering the **R**-Ω coupling and employing the correct angular basis $|J, M, \Omega\rangle$ for the initial state $|\,^1\Sigma\rangle$ with $|J^0_{^1\Sigma} = 0, M_{^1\Sigma} = 0, \Omega_{^1\Sigma} = 0\rangle$. It is worthwhile to note here that, for the $|\,^1\Pi\rangle$ initial (ground) state taking into account **R**-Ω coupling, an averaging over its six different initial angular states $[|J^0_{^1\Pi} = 1, M_{^1\Pi} = (0, \pm1), \Omega_{^1\Pi} = \Lambda_{^1\Pi} = (\pm1)\rangle]$ is required; if the initial state is a triplet $|^3\Sigma\rangle$, averaging over its nine degenerate initial angular states $[|J^0_{^3\Sigma} = 1, M_{^3\Sigma} = (0, \pm1), \Omega_{^3\Sigma} = \Sigma_{^3\Sigma} = (0, \pm1)\rangle]$ is required for the full treatment.

Figure 2(b) shows the variations of the upper state population after the pulse with respect to the Rabi frequency in the two different theoretical treatments. The difference between the conventional and full treatments is not very significant (see the black curve), having a periodical dependence with respect to the Rabi frequency and meeting the local maxima at full Rabi cycles. The conventional treatment has an about 10% inaccuracy compared with the improved treatment for $\Omega_{\text{Rabi}} = 0.52$ eV (≈3.0 Rabi cycles). Figure 2(c) illustrates details of the time-dependent dynamics of the upper state population for three selected values of the Rabi frequency $\Omega_{\text{Rabi}} =$ 0.01, 0.18, and 0.52 eV. The small difference in the electronic population shows that the **R**-Ω coupling does not affect very much the averaged electronic dynamics induced by the pulse. However, the degree of molecular alignment, presented in Fig. 2(d), is much more sensitive to the level of theory, and the difference between the two models is clearly visible already for $\Omega_{\text{Rabi}} \gtrsim 0.18$ eV (about one Rabi cycle). This is consistent with the fact that the **R**-Ω coupling directly affects the angular dependence of the transition matrix elements, especially for the upper $^1\Pi$ state. Besides the direct effect from the transition dipole moment (related to $\sin\beta$), the molecular rotations are also affected cumulatively for each electronic transition in connection with the γ angle and Ω angular momentum. This

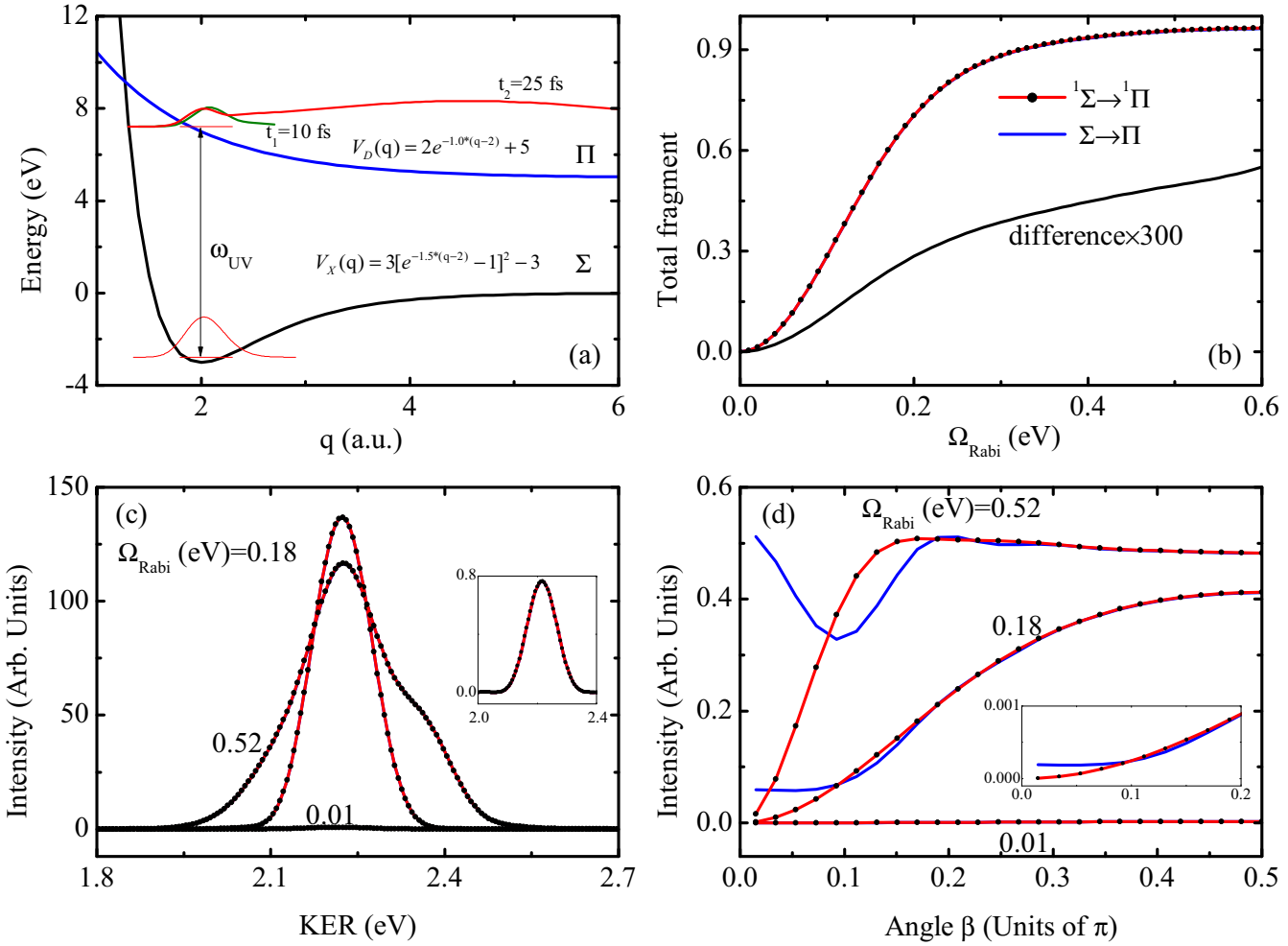

FIG. 3. (a) Potential-energy curves for the electronic transitions from the ground state $|^1\Sigma\rangle$ to a dissociative excited state $|^1\Pi\rangle$ and snapshots of the dissociative nuclear wave packets for $\Omega_{Rabi} = 0.52$ eV at $t_1 = 10$ and $t_2 = 25$ fs. (b) The total fragment yield simulated in the conventional ("$\Sigma - \Pi$," blue curve) and improved ("$^1\Sigma - {}^1\Pi$," red-dotted curve) theoretical treatments with respect to the Rabi frequency Ω_{Rabi}. The black curve shows the difference between the two models (results of the improved one minus the conventional one). (c), (d) The KER spectra and angular distribution of photofragments of the excited dissociative state for selected cases with $\Omega_{Rabi} = 0.01$, 0.18, and 0.52 eV, respectively.

illustrates the importance of the **R**-Ω coupling for an accurate account of the physical processes and quantities related to the molecular rotation and angular distributions. Note that the differences in the degree of alignment at the end of the laser pulse between the two models are about 15% and 11% for $\Omega_{Rabi} = 0.18$ and 0.52 eV, respectively; for a longer time of propagations, the overall difference becomes larger for the latter case.

The effect of **R**-Ω coupling in photodissociation processes coupled to molecular rotations is illustrated by considering the KER spectra and angular distributions of the photofragments, as shown in Figs. 3(b)–3(d). These figures reveal that both the total yield of photofragments and the KER spectra obtained by the two treatments with respect to Ω_{Rabi} do not present significant differences [see black curve in Fig. 3(b)]. For the intense case, $\Omega_{Rabi} = 0.52$ eV, both treatments predict that the total yield of photofragments reaches about 0.96 and the KER spectra split into double shoulders. It can be noted in passing that the peak splitting of KER spectra is a consequence of the interference between the photofragments appearing at different times during the laser pulse, similar to the effect observed in photoionization spectra in intense laser pulses [75].

The yield of photofragments is proportional to the population of the excited state, and the striking difference in the effect of the **R**-Ω coupling for the bound-bound [Fig. 2(b)] and bound-dissociative [Fig. 3(b)] transitions deserves a special mention. There are two main reasons for the much smaller effect in the latter case. First, the effective Rabi frequency of the molecular system is defined, in the Born-Oppenheimer approximation, by an electronic contribution Ω_{Rabi} multiplied by the nuclear part. The nuclear contribution to the transition dipole moment is the overlap of the ground- and excited-state vibrational wave functions (Franck-Condon factors), which are significantly different in the two discussed cases, being about 1 and much less than 1 for the bound-bound and bound-dissociative cases, respectively. This makes the effective Rabi frequency, and thus all strong-field effects, much smaller for the bound-dissociative transitions.

The second, but related, reason for a significantly smaller **R**-Ω-coupling effect in the bound-dissociative case as

compared with the bound-bound transition arises from the qualitatively different dynamics of the nuclear wave packet in these two cases. For the bound-bound case, the excited wave packet is confined near the equilibrium distance and is continuously driven by the intense pulse; the wave packet mostly remains in the Franck-Condon region during the pulse duration. In contrast, in the dissociative case, the wave packet quickly moves away from the Franck-Condon region, as illustrated in Fig. 3(a) for $\Omega_{\text{Rabi}} = 0.52$ eV, and so it escapes the region of overlap [see Fig. 3(a) of the wave packets at $t_2 = 25$ fs] with the ground-state wave function, thus suppressing the Rabi cycling driven by the laser pulse. Due to this, effectively only "a half" Rabi cycle takes place resulting in a much reduced effect in the total fragmentation yield and KER spectra.

In striking contrast with the small contribution of the **R**-Ω-coupling effect on the total fragmentation yield and KER spectra, the angular distribution of the photofragments shows a very significant difference between the two compared theoretical treatments, which is qualitatively different for small angles $\beta \leqslant 30^\circ$ between the laser polarization and the molecular axis [see Fig. 3(d)] . This is due to the fact that the evolution of the rotational wave packets depends strongly on the molecular rotation induced by the laser pulse with strong contribution from the effect of **R**-Ω coupling. The angular distribution presents also a much stronger modulation than the alignment discussed previously, because the latter is an averaged property. Indeed, the full treatment with **R**-Ω coupling has zero spectral intensity at $\beta = 0$ for any field amplitude, in contrast with the conventional treatment, which wrongly describes the increase of spectral intensity at small angles with the increase of the pulse intensity. This is in line with recent results that neglected the **R**-Ω coupling for MgH^+ [43]. The node at $\beta = 0$ is caused by the orthogonality between the electronic transition dipole moment from states $|\Sigma\rangle$ to $|\Pi\rangle$ with respect to the molecular axis, indicating that the transition element has to be zero at $\beta = 0$, which is in perfect agreement with the results of the improved theoretical treatment. Note that, in the weak-field limit, the intensity at small angles for the conventional model is not significant, so that the inaccuracy of the approximated description could be within the precision of measurements. For the interaction with intense laser fields of $\Omega_{\text{Rabi}} \gtrsim 0.18$ eV, the **R**-Ω coupling becomes of crucial importance: the ratio of the signal at $\beta = 0$ and $\beta = \pi/2$ varies from 10% and up to 100% when $\Omega_{\text{Rabi}} = 0.52$ eV obtained by the conventional treatment. Moreover, a significant dip appears around $\beta = 0.1\pi$, while the results with **R**-Ω coupling always exhibit a smooth sin-squared-like structure. These striking differences between the two models could be easily verified experimentally in a strong field to confirm the importance of considering the improved theoretical treatment discussed here. A field intensity of about 10^{12} W/cm^2 would be needed for a clear identification of the discussed effects, as can be estimated for the MgH^+ molecule considering that its transition dipole moment between the ground and valence excited states is about 1.0 a.u. [43].

IV. CONCLUSIONS

Photoexcitation and dissociation of diatomic molecules by intense pulse lasers have been very broadly investigated in the field of strong field physics. However, the question arises whether the conventionally and broadly employed theoretical treatment neglecting the **R**-Ω coupling breaks down in intense laser fields. To approach this question, a more general theoretical treatment has been introduced based on an angular basis of Wigner D functions and taking into account whether the electronic transition corresponds to $\Delta\Lambda = 0$ or ± 1. The usual case of photoinduced electronic transitions involving electronic states of $|^1\Sigma\rangle$ and $|^1\Pi\rangle$ symmetry was numerically investigated for the transitions to bound and dissociative excited states using both the conventional and the improved theoretical treatments. We showed that, when the field is strong enough to drive more than one Rabi cycle, the **R**-Ω-coupling effects become significant and the conventional treatment breaks down for some observables. In particular, the **R**-Ω coupling has a very strong effect on angular distributions of photofragments and it has a non-negligible effect on electronic populations and molecular alignment whenever there is a sustained interaction with the strong field that can accumulate over several Rabi cycles. This may have a potentially important impact in the description of the rotational dynamics of field-dressed states and in the description of light-induced conical intersections. As a means to verify the predicted effects experimentally, we propose considering, e.g., the angular distribution of photofragments or other suitable observables involving an excited $|^1\Pi\rangle$ state coupled to a ground $|^1\Sigma\rangle$ electronic state, both in bound and dissociative scenarios.

ACKNOWLEDGMENTS

S.B.Z. thanks H. D. Meyer for his helpful instructions of Wigner-DVR in MCTDH. Grants from the National Basic Research Program of China (2017YFA0403200), NSFC (No. 11604197, No. 11974230, and No. 11934004), the Science Challenge Program of China (TZ2018005 and TZ2016005) are acknowledged. V.K. acknowledges financial support from Swedish Research Council (VR) and the Ministry of Science and High Education of Russian Federation, Project No. FSRZ-2020-0008.

[1] J. H. Posthumus, Rep. Prog. Phys. **67**, 623 (2004).
[2] F. Krausz and M. Ivanov, Rev. Mod. Phys. **81**, 163 (2009).
[3] P. B. Corkum and F. Krausz, Nat. Phys. **3**, 381 (2007).
[4] K. W. D. Ledingham, P. McKenna, and R. P. Singhal, Science **300**, 1107 (2003).
[5] P. B. Corkum, Phys. Rev. Lett. **71**, 1994 (1993).
[6] H. J. Wörner, J. B. Bertrand, D. V. Kartashov, P. B. Corkum, and D. M. Villeneuve, Nature (London) **466**, 604 (2010).
[7] K. J. Schafer, B. Yang, L. F. DiMauro, and K. C. Kulander, Phys. Rev. Lett. **70**, 1599 (1993).
[8] S. Kim, J. Jin, Y.-J. Kim, I.-Y. Park, Y. Kim, and S.-W. Kim, Nature (London) **453**, 757 (2008).

[9] H. Stapelfeldt and T. Seideman, Rev. Mod. Phys. **75**, 543 (2003).

[10] M. Spanner, S. Patchkovskii, E. Frumker, and P. Corkum, Phys. Rev. Lett. **109**, 113001 (2012).

[11] A. S. Chatterley, C. Schouder, L. Christiansen, B. Shepperson, M. H. Rasmussen, and H. Stapelfeldt, Nat. Commun. **10**, 133 (2019).

[12] K. Lin, I. Tutunnikov, J. Qiang, J. Ma *et al.*, Nat. Commun. **9**, 5134 (2018).

[13] Y. Kobayashi, K. F. Chang, T. Zeng, D. M. Neumark, and S. R. Leone, Science **365**, 79 (2019).

[14] A. Kaldun, A. Blättermann, V. Stooß, S. Donsa *et al.*, Science **354**, 738 (2016).

[15] P. Peng, C. Marceau, M. Hervé, P. B. Corkum *et al.*, Nat. Commun. **10**, 5269 (2019).

[16] C. D. Lin and W.-C. Chu, Science **340**, 694 (2013).

[17] C. Ott, A. Kaldun, P. Raith, K. Meyer *et al.*, Science **340**, 716 (2013).

[18] S. B. Zhang, V. Kimberg, and N. Rohringer, Phys. Rev. A **94**, 063413 (2016).

[19] W. Zhang, X. Gong, H. Li *et al.*, Nat. Commun. **10**, 757 (2019).

[20] P. Lu, J. Wang, H. Li *et al.*, Proc. Natl. Acad. Sci. USA **115**, 2049 (2018).

[21] M. F. Kling, C. Siedschlag, A. J. Verhoef *et al.*, Science **312**, 246 (2006).

[22] E. Goulielmakis, Z.-H. Loh, A. Wirth *et al.*, Nature (London) **466**, 739 (2010).

[23] C. Brif, R. Chakrabarti, and H. Rabitz, New J. Phys. **12**, 075008 (2010).

[24] C. Bostedt, S. Boutet, D. M. Fritz, Z. Huang *et al.*, Rev. Mod. Phys. **88**, 015007 (2016).

[25] B. W. J. McNeil and N. R. Thompson, Nat. Photonics **4**, 814 (2010).

[26] J. Ullrich, A. Rudenko, and R. Moshammer, Annu. Rev. Phys. Chem. **63**, 635 (2012).

[27] K. Zhao, Q. Zhang, M. Chini, Y. Wu, X. Wang, and Z. Chang, Opt. Lett. **37**, 3891 (2012).

[28] E. Allaria, R. Appio, L. Badano *et al.*, Nat. Photonics **6**, 699 (2012).

[29] L. Young, K. Ueda, M. Gühr *et al.*, J. Phys. B: At., Mol. Opt. Phys. **51**, 032003 (2018).

[30] J. Duris, S. Li, T. Driver *et al.*, Nat. Photonics **14**, 30 (2020).

[31] M. E. Corrales, R. de Nalda, and L. Bañares, Nat. Commun. **8**, 1345 (2017).

[32] N. Saito, H. Sannohe, N. Ishii *et al.*, Optica **6**, 1542 (2019).

[33] F. Kelkensberg, C. Lefebvre, W. Siu, O. Ghafur, T. T. Nguyen-Dang, O. Atabek, A. Keller, V. Serov, P. Johnsson, M. Swoboda *et al.*, Phys. Rev. Lett. **103**, 123005 (2009).

[34] M. S. Schöffler, J. Titze, N. Petridis *et al.*, Science **320**, 920 (2008).

[35] P. V. Demekhin, S. D. Stoychev, A. I. Kuleff, and L. S. Cederbaum, Phys. Rev. Lett. **107**, 273002 (2011).

[36] G. A. Worth and L. S. Cederbaum, Annu. Rev. Phys. Chem. **55**, 127 (2004).

[37] S. Matsika and P. Krause, Annu. Rev. Phys. Chem. **62**, 621 (2011).

[38] J. E. Bækhøj, C. Lévêque, and L. B. Madsen, Phys. Rev. Lett. **121**, 023203 (2018).

[39] M. Kowalewski, K. Bennett, K. E. Dorfman, and S. Mukamel, Phys. Rev. Lett. **115**, 193003 (2015).

[40] M. Kowalewski, B. P. Fingerhut, K. E. Dorfman *et al.*, Chem. Rev. (Washington, DC, U.S.) **117**, 12165 (2017).

[41] M. E. Corrales, J. González-Vázquez, G. Balerdi *et al.*, Nat. Chem. **6**, 785 (2014).

[42] A. Tóth, A. Csehi, G. J. Halász, and A. Vibók, Phys. Rev. A **99**, 043424 (2019).

[43] P. Badankó, G. J. Halász, L. S. Cederbaum, A. Vibók, and A. Csehi, J. Chem. Phys. **149**, 181101 (2018).

[44] R. Tehini, M. Z. Hoque, O. Faucher, and D. Sugny, Phys. Rev. A **85**, 043423 (2012).

[45] B. A. Zon and B. G. Katsnelson, Sov. Phys. Opt. Spectr **40**, 544 (1976).

[46] N. B. Delone, V. P. Krainov, and E. Yankovsky, *Atoms in Strong Light Fields*, Springer Series in Chemical Physics (Springer, New York, 1985).

[47] R. N. Zare, *Angular Momentum: Understanding Spatial Aspects in Chemistry and Physics* (John Wiley & Sons, New York, 1988).

[48] H. Lefebvre-Brion and R. W. Field, *The Spectra and Dynamics of Diatomic Molecules: Revised and Enlarged Edition* (Elsevier, New York, 2004).

[49] E. E. Whiting and R. W. Nicholls, Astrophys. J., Suppl. Ser. **27**, 1 (1974).

[50] M. Beck, A. Jackle, G. Worth, and H.-D. Meyer, Phys. Rep. **324**, 1 (2000).

[51] B. A. Zon and E. I. Sholokhov, Sov. Phys. JETP **70**, 887 (1976).

[52] X. Shi, Y. Wu, J. G. Wang, V. Kimberg, and S. B. Zhang, Phys. Rev. A **101**, 023401 (2020).

[53] Q. Bian, Y. Wu, J. G. Wang, and S. B. Zhang, Phys. Rev. A **99**, 033404 (2019).

[54] O. I. Tolstikhin, T. Morishita, and L. B. Madsen, Phys. Rev. A **84**, 053423 (2011).

[55] A. S. Kornev, I. M. Semiletov, and B. A. Zon, Laser Phys. **26**, 055302 (2016).

[56] K.-P. Huber, *Molecular Spectra and Molecular Structure: IV. Constants of Diatomic Molecules* (Springer Science & Business Media, New York, 2013).

[57] L. Holmegaard, J. H. Nielsen, I. Nevo, H. Stapelfeldt, F. Filsinger, J. Küpper, and G. Meijer, Phys. Rev. Lett. **102**, 023001 (2009).

[58] S. J. Weber, M. Oppermann, and J. P. Marangos, Phys. Rev. Lett. **111**, 263601 (2013).

[59] P. M. Kraus, S. B. Zhang, A. Gijsbertsen, R. R. Lucchese, N. Rohringer, and H. J. Wörner, Phys. Rev. Lett. **111**, 243005 (2013).

[60] R. N. Zare, Mol. Photochem. **4**, 1 (1972).

[61] M. Šindelka and N. Moiseyev, J. Phys. Chem. A **110**, 5561 (2006).

[62] A. Brown and G. G. Balint-Kurti, J. Chem. Phys. **113**, 1870 (2000).

[63] P. V. Demekhin and L. S. Cederbaum, J. Phys. B: At., Mol. Opt. Phys. **46**, 164008 (2013).

[64] P. V. Demekhin, Y.-C. Chiang, and L. S. Cederbaum, Phys. Rev. A **84**, 033417 (2011).

[65] J. F. Triana and J. L. Sanz-Vicario, Phys. Rev. Lett. **122**, 063603 (2019).

[66] A. Tóth, P. Badankó, G. J. Halász, Ágnes Vibók, and A. Csehi, Chem. Phys. **515**, 418 (2018).

[67] C.-C. Shu, K.-J. Yuan, D. Dong *et al.*, J. Phys. Chem. Lett. **8**, 1 (2017).

[68] A. Tóth, A. Csehi, G. J. Halász, and A. Vibók, Phys. Rev. Research **2**, 013338 (2020).

[69] L. S. Cederbaum, Y.-C. Chiang, P. V. Demekhin, and N. Moiseyev, Phys. Rev. Lett. **106**, 123001 (2011).

[70] Z. Sun, C. Wang, W. Zhao, and C. Yang, J. Chem. Phys. **149**, 224307 (2018).

[71] C. Buth, Chem. Phys. **518**, 91 (2019).

[72] S. C. Rand, *Lectures on Light: Nonlinear and Quantum Optics Using the Density Matrix* (Oxford University Press, Oxford, 2016).

[73] G. A. Worth, M. H. Beck, A. Jäckle, O. Vendrell, and H.-D. Meyer, The MCTDH Package, Version 8.2, (2000); H.-D. Meyer, Version 8.3 (2002), Version 8.4 (2007); O. Vendrell and H.-D. Meyer Version 8.5 (2013); Version 8.5 contains the ML-MCTDH algorithm. Current versions: 8.4.18 and 8.5.11 (2019). Used version: exchange with "Used version." See http://mctdh.uni-hd.de/.

[74] G. J. Halász, A. Vibók, N. Moiseyev, and L. S. Cederbaum, Phys. Rev. A **88**, 043413 (2013).

[75] P. V. Demekhin and L. S. Cederbaum, Phys. Rev. Lett. **108**, 253001 (2012).